UDK 66.065.32-026.652:539.56:549.2
Original scientific article/Izvirni znanstveni članek

ISSN 1580-2949
MTAEC9, 58(3)285(2024)

EFFECT OF LONG-TERM THERMAL AGING AT 475 °C ON EMBRITTLEMENT OF Fe-32Cr-4Ni-4Cu MODEL ALLOY

VPLIV DOLGOTRAJNEGA TERMIČNEGA STARANJA PRI 475 °C NA KRHKOST MODELNE ZLITINE Fe-32Cr-4Ni-4Cu

Xiaoming Du[1], Zhendong Sun[1], Xue Ma[1], Ming Ma[1*], ZhijunWang[2], Tianfu Li[2]

[1]School of Materials Science and Engineering, Shenyang Ligong University, Shenyang 110159, China
[2]China Institute of Atomic Energy, Beijing 102413, China

Prejem rokopisa – received: 2023-11-10; sprejem za objavo – accepted for publication: 2024-03-13

doi:10.17222/mit.2023.1044

The microstructure evolution and mechanical properties of a Fe-32Cr-4Ni-4Cu model alloy after long-term thermal aging at 475 °C was investigated in this study. The spinodal decomposition of the model alloy during thermal aging and the crystal structure evolution of Cu-rich precipitates were observed and analyzed using high-resolution transmission electron microscopy (TEM). It was revealed that after long-term thermal aging, the crystal structure of the precipitated Cu-rich phases in the Fe-32Cr-4Ni-4Cu model alloy transformed from a BCC structure to a multi-twin 9R or 2H structure, ultimately transforming into a stable FCC structure. During long-term thermal aging at 475 °C, the precipitated Cu-rich phase and the Cr-rich α'-phase produced by spinodal decomposition cause an increase in the hardness of the model alloy. The hardness of the model alloy in the early stage of thermal aging greatly depends on the Cu-rich precipitates. After continuous thermal aging for 1000 h, the hardness of the alloy depends on the Cr-rich α'-phase. The results of an oscillographic impact test indicate that the fracture mechanism of the model alloy after thermal aging at 475 °C is brittle fracture, which is mainly influenced by the precipitation of Cu-rich phases during the thermal aging process.

Keywords: model alloy, thermal aging, spinodal decomposition, Cu-rich precipitate, fracture mechanism

V članku avtorji opisujejo študijo razvoja mikrostrukture in mehanskih lastnosti modelne zlitine Fe-32Cr-4Ni-4Cu po dolgotrajnem staranju pri 475 °C. Avtorji so opazovali proces spinodalnega razpada (dekompozicije) izbrane modelne zlitine in razvoj kristalne strukture izločkov bogatih na bakru (Cu) in kromu (Cr) med termičnim staranjem. Analize so izvajali s pomočjo presevnega elektronskega mikroskopa z visoko ločljivostjo (HRTEM). Ugotovili so, da se po dolgotrajnem termičnem staranju kristalna struktura izločkov na bakru bogatih faz modelne zlitine Fe-32Cr-4Ni-4Cu pretvori iz prostorsko centrirane kubične strukture (BCC) v mnogo-dvojčično 9R ali 2H in nato dokončno v stabilno ploskovno centrirano kubično (FCC) strukturo. Izločene na bakru bogate faze in na kromu bogata faza α', nastale med dolgotrajnim termičnim staranjem modelne zlitine pri 475 °C povzročijo povišanje njene trdote. Trdota modelne zlitine je v začetnih stadijih staranja močno odvisna od deleža in velikosti na bakru bogatih izločkov. Po 1000 urnem kontinuirnem staranju pa je trdota modelne zlitine odvisna od na kromu bogate faze α'. Rezultati oscilografskih testov žilavosti so pokazali, da je po termičnem staranju pri 475 °C prišlo do krhkega loma oziroma krhkega mehanizma porušitve v glavnem zaradi nastanka izločkov na Cu bogatih faz, ki so nastale med spinodalnim razpadom.

Keywords: modelna zlitina, termično staranje, spinodalni razpad, izločki bogati na bakru, mehanizem porušitve

1 INTRODUCTION

Martensitic precipitation-hardening stainless steel is a kind of steel with higher strength than martensitic stainless steel. This is achieved by adding Cu, Mo, Ti, Al and other elements with a precipitation-hardening effect to the base martensitic stainless steel. In combination with C, N and other elements in the steel, these additions form a precipitation-hardening phase or intermetallic compound. The carbon content is less than 0.1 %. At present, the common and widely used martensitic precipitation-hardening stainless steels include 15-5PH stainless steel, 17-4PH stainless steel, etc. 17-4PH stainless steel (0Cr17Ni4Cu4Nb), as a typical representative of martensitic precipitation-hardening stainless steel, is widely used in aerospace, nuclear industry, energy and other fields because of its outstanding mechanical properties, good corrosion resistance and good high-temperature performance.[1,2] Domestic and foreign scholars mainly focus on the effect of thermal-aging behavior on its microstructural and mechanical properties, and thoroughly study the spinodal decomposition mechanism of ferrite during thermal aging of 17-4PH stainless steel as well as characterizing and analyzing the second phase produced during thermal aging.

When a Fe-Cr alloy is used in a temperature range of 300–600 °C, it decomposes into a Cr-rich α' phase and Fe-rich α phase, causing a lattice distortion of the matrix, and resulting in material embrittlement.[3] For the Fe-Cr-Ni-Cu alloy, the nano-Cu-rich phase precipitated during thermal aging is the main precipitate that causes the alloy to harden. Therefore, many scholars have conducted in-depth research on the Cu-rich phase precipitated in the alloy matrix, the mechanism of spinodal decomposition and its products. J. Wang et al. studied the long-term aging of 17-4PH stainless steel at 350 °C and

*Corresponding author's e-mail:
neummslq@126.com (Ming Ma)

found that when the aging time is 12 months, the α' phase decomposition is produced and precipitated, enhancing the hardness of the alloy.[4] During a thermal-aging reaction of 17-4PH stainless steel, C. N. Hsiao and others observed, through a transmission electron microscope, that copper precipitates were precipitated in the sample after aging at 480 °C for 1 h.[5] Zou Hong et al. observed the microstructure of 17-4PH stainless steel after long-term aging at 350 °C under a transmission electron microscope, and found that the spinodal decomposition first occurred at the grain boundaries and then, with the aging time, the grain-boundary spinodal decomposition gradually changed into the intragranular decomposition, while the G phase and sigma phase could also be observed.[3] However, within the investigation of the nano-Cu-rich phase, spinodal decomposition mechanism and their products, there are few studies on the effect of the thermal-aging time on the microstructure of the Cu-rich phase and spinodal decomposition products.

A Fe-32Cr-4Ni-4Cu model alloy was designed in this work. The change in the microstructure of the nano-Cu-rich phase precipitated from the alloy matrix, the mechanism of spinodal decomposition and the microstructure of the product were mainly studied during the thermal aging of the model alloy for 1000 h at 475 °C. The effect of the Cu-rich phase and spinodal decomposition on the mechanical properties of the alloy was analyzed with a microhardness and oscillographic impact test.

2 EXPERIMENTAL PART

2.1 Materials and the heat treatment process

Based on the phase diagram of the Fe-Cr binary alloy and the alloy composition of 17-4PH stainless steel, the Fe-32Cr-4Ni-4Cu model alloy was designed to study the mechanism of spinodal decomposition of the Fe-Cr-Ni-Cu model alloy and the mechanism of precipitation embrittlement of the Cu-rich phase. The alloy is made of high-purity Fe (99.9 *w*/%), Cr (99.99 *w*/%), Cu (99.99 *w*/%) and high-purity nickel (99.98 *w*/%) by melting them at a high temperature. Its specific chemical composition is shown in **Table 1**.

Table 1: Chemical composition of Fe-32Cr-4Ni-4Cu model alloy (*w*/%)

Alloying element	Fe	Cr	Ni	Cu
Element content	59.7	32.0	4.8	3.5

The high-purity materials (99.9 *w*/% Fe, 99.99 *w*/% Cr, 99.99 *w*/% Cu and 99.98 *w*/% Ni) are melted and cast into ingots in a vacuum induction furnace; the ingots are homogenized at 1175 °C for 3h; then the ingots are hot forged into 40-mm thick slabs at 900–1150 °C; then they are hot rolled at 1000 °C, and finally made into 15-mm thick strips with multi-pass rolling. The hot-rolled strips are cut into (15 × 15 × 9.5) mm blocks, vacuum sealed in a quartz tube, heated to 1050 °C for 2 h, and then quenched in saturated salt water. The model alloy sample after solution quenching is subjected to thermal aging for (100, 300, 500 and 1000) h at 475 °C.

2.2 Structure and performance characterization

The products of the spinodal decomposition, precipitation morphology and the crystal structure of the Cu-rich phase of the model alloy for different thermal-aging times were observed using a high-resolution transmission electron microscope (JEOL JEM-2100F). A Rigaku Ultima IV X-ray diffractometer was used to carry out phase identification and a quantitative analysis of the model alloy, study the atomic scale structure of the alloy, and set the diffraction angle (2θ). The range was 20–100°. The original XRD data were refined and analyzed using the MDI Jade 6.0 program. The fracture of the impact sample was observed with a Hitachi S-3400N scanning electron microscope (SEM).

Mechanical properties of the specimens with and without aging were determined by Charpy V-notch impact tests, and Vickers hardness tests at room temperature. (10 × 10 × 55) mm specimens with a 2 mm V-notch in accordance with the ASTM E23 standard were tested on an instrumented 300J Charpy impact testing machine. Hardness tests were made using a Vickers hardness tester (with a load of 1 kg applied for 15 s). Hardness measurements were periodically obtained throughout the aging process, and the aging continued until the hardness stopped increasing.

3 RESULTS AND DISCUSSION

3.1 Microstructure evolution during thermal aging

Figure 1 shows the TEM morphology of the model alloy after its heat aging for 300 h at 475 °C. The substructure morphology of the flat-noodle martensite structure in the matrix is shown in **Figure 1a**. In addition, there is a large amount of dispersed nano-Cu-rich phases. **Figure 1b** is a locally enlarged view of **Figure 1a**. It can be observed that a large number of dislocations are distributed across the martensitic matrix. The dislocations are intertwined with each other, and there are more Cu-rich phases precipitated at the dislocations and flat-noodle martensite grain boundaries. This is because during the thermal-aging process, as the aging time prolongs, the internal structure of the alloy is in an unstable state. In order to restore it to a stable state, there are energy fluctuations in the model alloy system. Especially, the energy fluctuations at the dislocations and grain boundaries are significant, as they are conducive to the nucleation and growth of Cu-rich phases, resulting in the generation of more nano-Cu-rich phases at these two positions.[6] Electron diffraction spots obtained after the Fourier transform (FFT) of the martensite structure are calibrated as shown in the lower right-hand corner of

Figure 1b. It is a BCC structure with a lattice constant of 0.26 nm.

On **Figure 1c**, it can be observed that there are black and white layered structures at the grain boundaries (as indicated by the white arrows), the products of spinodal decomposition of the martensitic matrix during thermal aging. The EDS detection of this area found that the white area is a Fe-enriched BCC phase (α), while the black area is a Cr-enriched BCC phase (α'). This result is consistent with the result for the microstructure of 17-4PH stainless steel after long-term aging at 350 °C obtained by Zou et al.[3] The alternating black and white regions from **Figure 1d** may have been formed due to lattice distortion, leading to different diffraction contrasts when the electron beam passes through a thin film sample. The interface between the α and α' phases is fuzzy, indicating that the spinodal decomposition in ferrite did not reach equilibrium after aging at 475 °C for 300 h, which is in the early stage. Diffraction spots have the characteristics of typical satellite spots in spinodal decomposition.

Figure 2 shows micrographs of the spinodal decomposition structure in certain areas after thermal aging for 1000 h, as well as HRTEM and electron diffraction patterns of the corresponding areas. Compared with the thermal aging at 475 °C for 300 h (**Figure 1c**), spinodal decomposition in the martensitic matrix is more abundant at this time, and the position of occurrence shifts from grain boundaries to grains. The position indicated by the white arrow in **Figure 2a** can be clearly seen at the phase interface α-α'. The two-phase structure is distributed in black and white stripes. The calibration of diffraction points after the FFT transformation is shown in the bottom right-hand corner of **Figure 2b**. A diffraction spot has typical satellite spot characteristics. The appearance of satellite spots indicates the existence of micro regions with different lattice parameters in ferrite, namely solute-poor and solute-rich regions, which further indicates the occurrence of spinodal decomposition in the crystal.[7] However, after thermal aging for 1000 h at 475 °C, the aging time is still shorter than the actual service time, and the spinodal decomposition is still continuing, not reaching the stable stage. The high surface energy at the grain boundaries and active atomic motion are beneficial for the spinodal decomposition. Therefore, spinodal decomposition begins at the grain boundaries. The products of spinodal decomposition are two alternating lamellar structures. The reasons for these lamellar

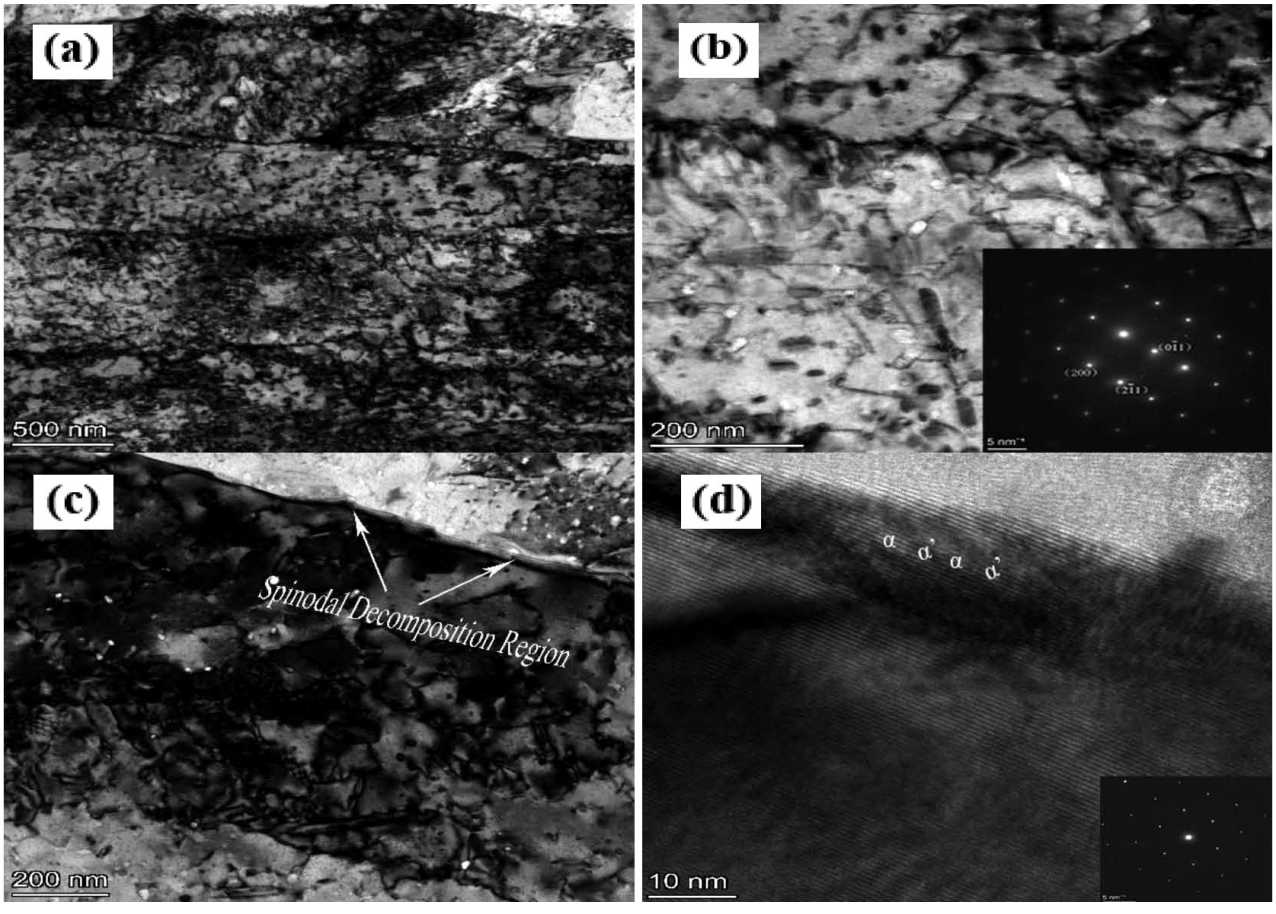

Figure 1: TEM images of the model alloy aged at 475 °C for 300 h: a) microstructure of lath martensite, b) local enlargement and the corresponding diffraction spots, c) image of the spinodal decomposition structure (arrowed), d) HRTEM and diffraction spots in the spinodal decomposition region

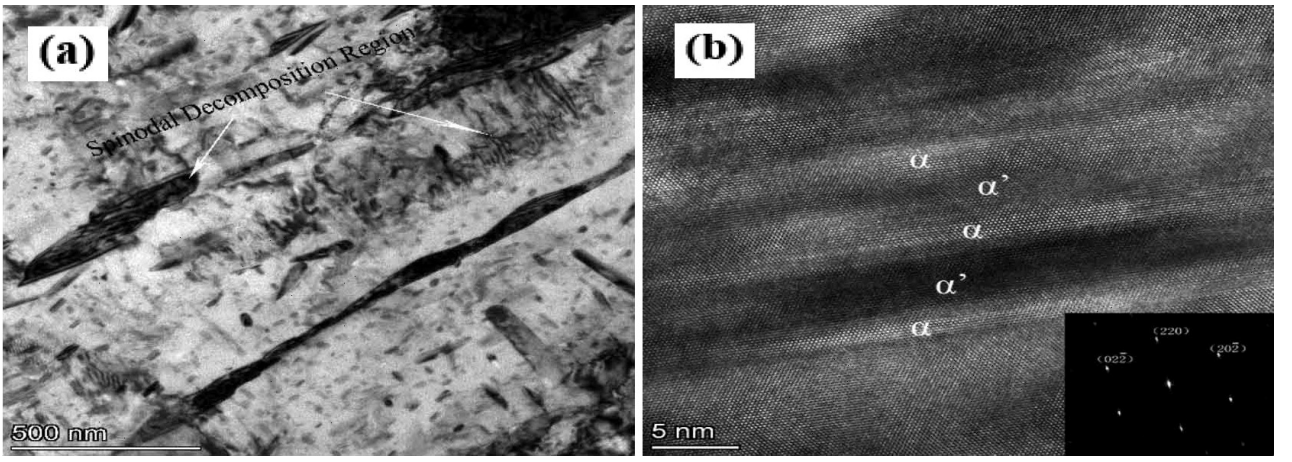

Figure 2: TEM images of the model alloy aged for 1000 h at 475 °C: a) spinodal decomposition region, b) HRTEM and diffraction spots in the spinodal decomposition region

structures may have been different materials and heat-treatment conditions. [8]

For the precipitation-hardened stainless steel, the nano-Cu-rich phase plays a major role in strengthening the stainless steel during thermal aging, and has a significant impact on the mechanical properties of the alloy. Due to the complexity and variability of the precipitation process and crystal structure evolution, extensive research was conducted on them. **Figure 3** is a TEM micrograph of the nano-Cu-rich phase precipitated from the model alloy after thermal aging at 475 °C for 300 h. On **Figure 3a**, it can be observed that the nano-Cu-rich phase is mainly distributed in the spherical shape at the dislocations after thermal aging for 300 h, with a size of

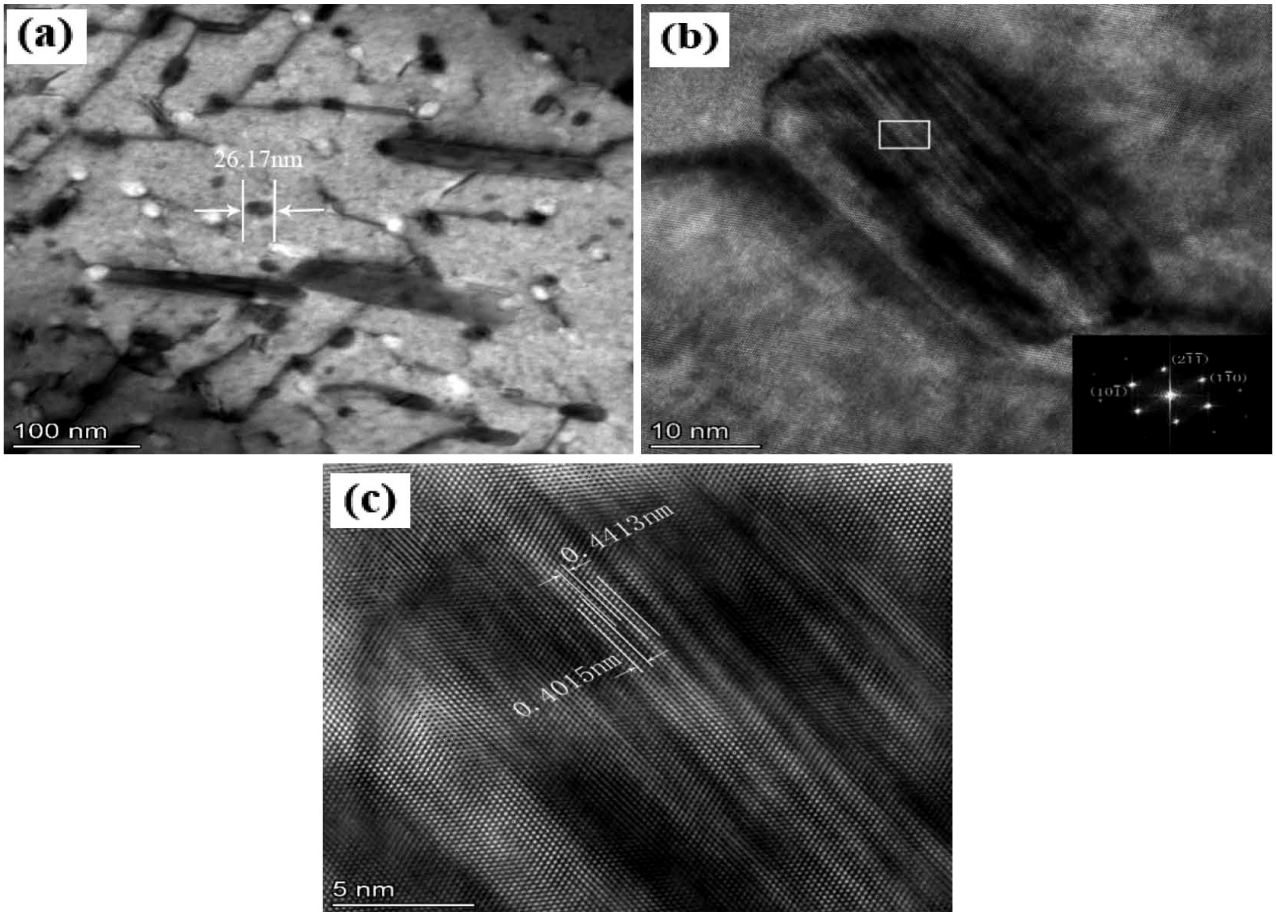

Figure 3: TEM images of the Cu-rich phase after aging at 475 °C for 300 h; a) HRTEM of Cu precipitates, b) HRTEM and diffraction spots of the Cu-rich phase, c) IFFT of (b)

about 25–30 nm. The diffraction spot shown in the lower right-hand corner is obtained with the FFT transformation of the white box position in **Figure 3b**. After calibration, it is found that its crystal structure is the BCC structure, indicating that it is in the initial stage of formation of the nano-Cu-rich phase.[9] **Figure 3c** is obtained by inverse Fourier transform (IFFT) of the diffraction pattern from **Figure 3b**. It can be found that there are atomic planes with three layers of atoms as the period. The atomic plane with a brighter contrast was observed to be the Cu atomic plane, with a crystal plane spacing of approximately 0.4015 nm, while the crystal plane spacing between the two layers with a darker contrast was 0.4413 nm. The crystal plane spacing of α-Fe is very close. The reason for this is that the atomic planes with different contrasts in the lattice stripes may be related to the segregation of different atoms on the crystal plane.[10]

Figure 4 shows TEM images of the Cu-rich phase precipitated from the model alloy after thermal aging at 475 °C for 1000 h. When the thermal aging time is extended to 1000 h, as shown in **Figure 4a**, the precipitated Cu-rich phase gradually changes from spherical to ellipsoidal and short rod-shaped, and its size is significantly larger than that of the Cu-rich phase precipitated at 475 °C for 300 h, which is about 48.55 nm. When the model alloy is aged at 475 °C for 1000 h, the high-resolution pattern of the precipitated nano-Cu-rich phase shows more fringes in different directions. According to the direction of the fringes, it can be divided into three regions, as shown in **Figure 4b**. The electron diffraction patterns shown in **Figures 4c** and **4d** are obtained with the Fourier transform of Regions 2 and 3, respectively. The longer the thermal aging time, the more complex the crystal structure of the precipitated Cu-rich phase may be.

Liu et al. found that the same Cu-rich phase may be composed of many different crystal structures and distributed across different regions when characterizing the complex crystal structure of a nanocrystalline Cu-rich precipitated phase.[11] When studying the precipitation of Cu-rich phase clusters, Wang et al. also showed that the precipitated Cu-rich phase structure can be formed by

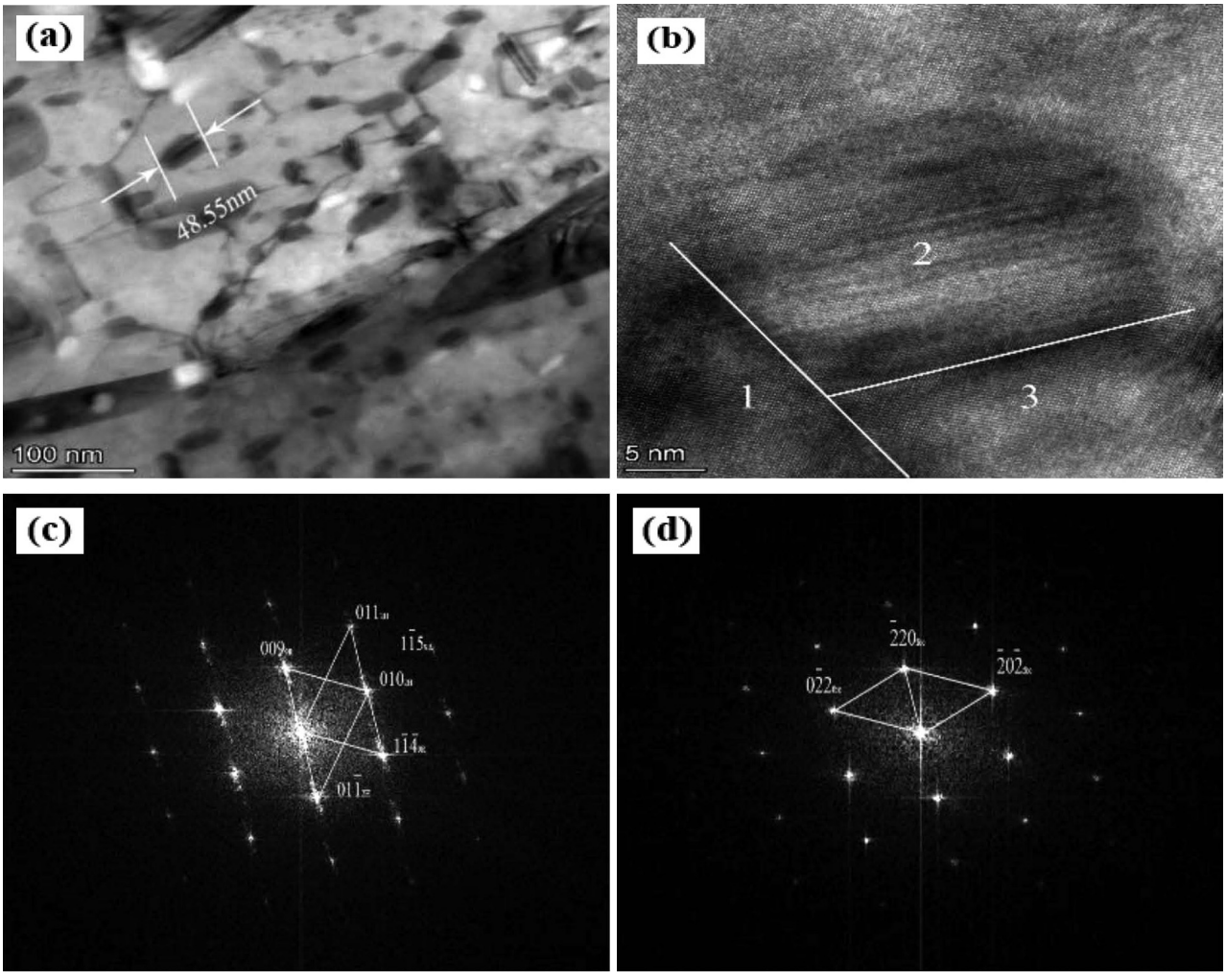

Figure 4: TEM images of the Cu-rich phase after aging for 300 h at 475 °C: a) HRTEM micrograph, b) HRTEM and diffraction spots of the Cu-rich phase, c) diffraction spots in Region 2 of **Figure b**, d) diffraction spots in Region 3 of **Figure b**

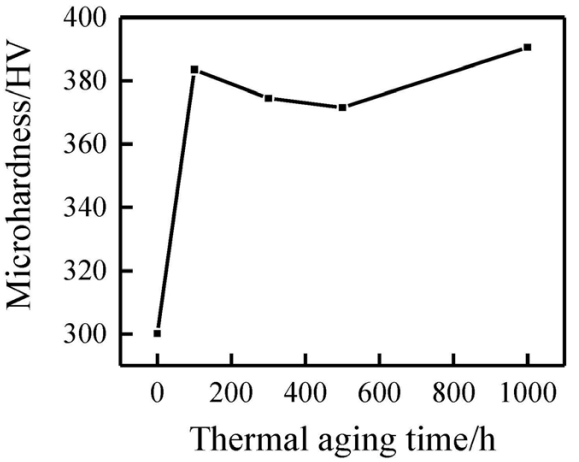

Figure 5: Hardness of the model alloy after heat aging at 475 °C for different times

stacking many 9R, 2H or FCC thin layer structures.[12] After the calibration of the electron diffraction spots, it was found that there were two sets of diffraction spots in Area 2, corresponding to **Figure 4b**. After the calibration, it was found that the Cu-rich phase crystal structure in this area was a mixture of 9R and 2H close-packed structures, which was basically consistent with the results found by Liu et al. and Wang et al. The diffraction spot obtained after the Fourier transform (FFT) of Region 3 is shown in **Figure 4c**. After calibration, it was found that the structure of the Cu-rich phase in this region was the FCC structure, further confirming the views of the two individuals mentioned above.

3.2 Heat-aging hardening behavior

Figure 5 shows the microhardness curve of the Fe-32Cr-4Ni-4Cu model alloy after thermal aging at 475 °C for different times. The value at 0 represents the hardness value of the model alloy after the solution treatment and saturated salt water quenching. It can be seen on **Figure 5** that the alloy shows a significant precipitation-hardening behavior during thermal aging at 475 °C. When the thermal aging time is extended from 0 to 100 h, the hardness of the alloy increases greatly from 300.2 HV to 383.5 HV. It is indicated that the Cu-rich phase begins to precipitate after 100 h of thermal aging. At this time, the size of the precipitated phase is small but the number is large, and the dispersed distribution in the matrix hinders the slip of dislocation, resulting in a rapid increase in the hardness of the model alloy. When the thermal aging time increases from 100 h to 500 h, the hardness is slightly decreased. This is due to the aggregation and coarsening of the precipitated Cu-rich phase, resulting in its precipitation hardening effect to decrease. After 500 h, the hardness increases. This indicates that the Cu-rich phase precipitated from the model alloy during thermal aging at 475 °C plays a major role in precipitation hardening. But beyond that, the ferrite phase of the model alloy undergoes spinodal decomposition during thermal aging at 475 °C. This has an impact on the hardening behavior of the alloy. When the thermal aging time reaches 300 h, spinodal decomposition begins to occur, resulting in a small amount of embrittlement. The α' phase has little effect on the hardness of the alloy. When the thermal aging time is up to 1000 h, the spinodal de-

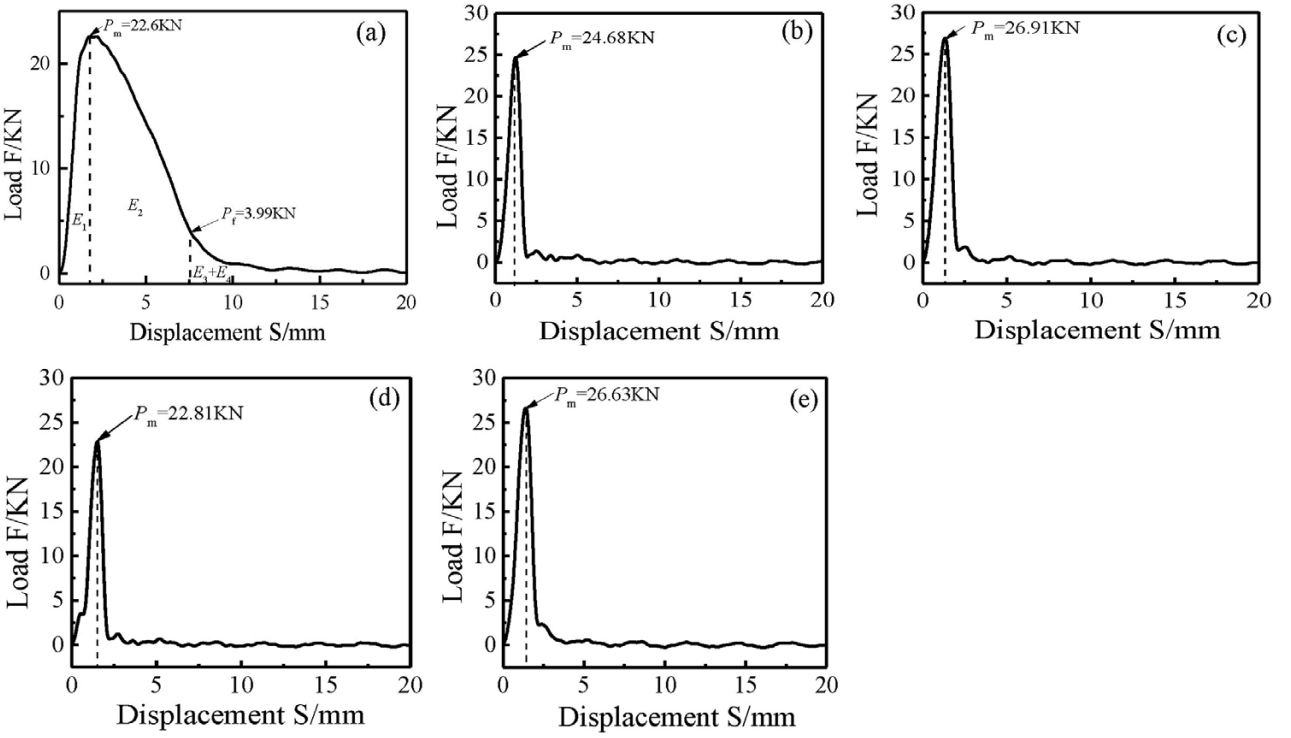

Figure 6: Impact curves of the model alloy aged at 475 °C: a) without aging, b) 100 h, c) 300 h, d) 500 h, e) 1000 h

composition in the model alloy occurs from the grain boundaries to the interior of the grains, thus it is more fully carried out. The increase in the α' phase causes the alloy to harden, resulting in a further increase in the hardness.

3.3 Oscillographic shock test results

Figure 6 shows the load-displacement impact curves of the model alloy after thermal aging at 475 °C for different times. **Figure 6a** shows the impact curve of the model alloy after thermal-aging treatment. It can be seen that the curve is a typical ductile impact curve. The difference between the maximum impact load P_m and the brittle fracture starting load P_f ($P_m - P_f$ = 18.61kN) is large, indicating that the model alloy has a small tendency to brittle fracture and good impact toughness. Although the matrix of the model alloy undergoes a solid-solution treatment to form a martensitic structure with high-density dislocations, it is mainly block martensite with larger martensite spacing. There is no precipitation hardening phase in the matrix, and the solid-solution strengthening effect is relatively small. Therefore, the toughness of the alloy is good. **Figures 6b** to **6e** show the oscillographic impact curves of the model alloy after thermal aging at 475 °C for 100–1000 h. It can be found that these curves are typical brittle-fracture impact curves. The shape of the load-displacement curves of the alloy is relatively steep. The maximum impact load P_m that the alloy can withstand during thermal aging does not change with the aging time. Before reaching the maximum force, the elastic deformation work accounts for a large proportion. After reaching the maximum load, the curves show a precipitous downward

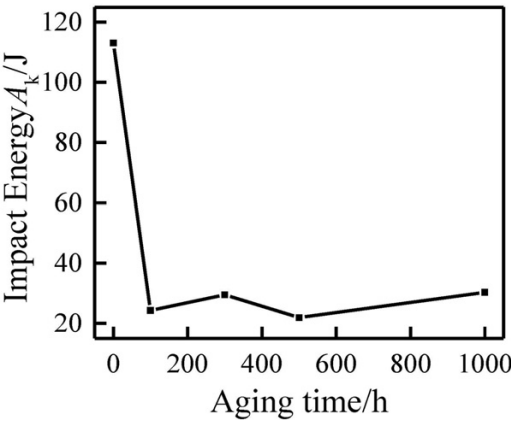

Figure 7: Impact-absorption energy of the model alloy after thermal aging at 475 °C

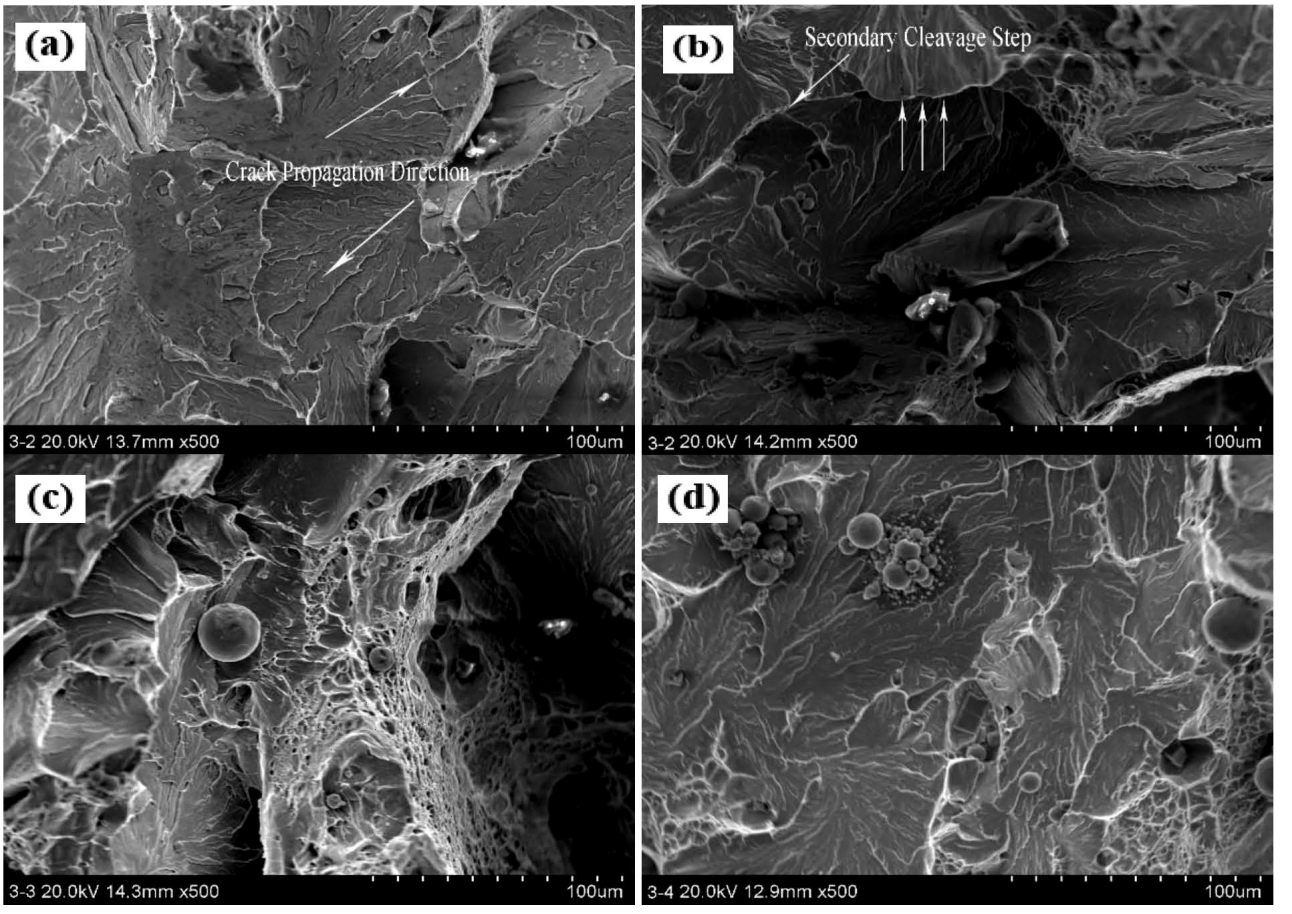

Figure 8: Impact-fracture morphology of the model alloy at 475 °C after different thermal-aging times: a) 100 h, b) 300 h, c) 500 h, d) 1000 h

trend, and the crack-propagation work is almost zero. This shows that the model alloy basically does not undergo any plastic deformation before fracture. When a crack is formed and it continues to be subjected to an external force, the crack expands rapidly in the structure until the alloy breaks, making the model alloy more prone to brittle fracture.[13]

Figure 7 shows the curve of the impact absorption energy of the model alloy after thermal aging at 475 °C for different times, where the value at 0 represents the impact energy of the model alloy after the solution treatment and saturated salt water quenching, and its value is 113.11 J. Due to the absence of precipitation-hardening phases in the alloy matrix without thermal aging treatment, the alloy has good toughness and large impact-absorption energy. After thermal aging, the impact energy of the alloy is lower than that of the alloy without thermal aging, and it fluctuates slightly with the extension of the thermal-aging time. During the thermal-aging process, there is precipitation of the Cu-rich phases in the model alloy, which plays a precipitation-hardening role in the alloy, leading to a rapid increase in the alloy hardness, increased brittleness, and weakened damage resistance. Therefore, the impact-absorption energy during the impact process is relatively small. During the thermal-aging process at 475 °C, the impact toughness of the alloy is affected by the accumulation and growth of Cu-rich phases in the alloy, as well as the spinodal decomposition. Therefore, the impact-absorption energy fluctuates, but the change is not significant.

Figure 8 shows the impact-fracture morphology of the model alloy at 475 °C for different times. It can be seen that the alloy exhibits a typical brittle-fracture morphology, being mainly of the river type. The fracture morphology of the alloy after different times of thermal aging basically has a "continuous" river shape, and the directions of crack propagation are shown by the arrows in **Figures 8a** and **8b**, which are consistent with the flow direction of the river.[14] When the thermal aging time is 500 h, as shown in **Figure 8c**, a small number of shallow ductile dimples appear on the fracture surface, and the size is relatively small, indicating that the toughness of the alloy has an increasing trend compared to the other thermal-aging times. The model alloy undergoes a transition from ductile fracture without thermal aging to brittle fracture after aging, indicating that the alloy undergoes thermal-aging embrittlement at 475 °C, resulting in high hardness and poor toughness. This is because during the thermal-aging process at 475 °C, Cu-rich and Cr-rich phases are generated in the matrix of the model alloy. These two phases enhance the matrix and cause the material to harden, thereby reducing the impact toughness of the model alloy.

4 CONCLUSION

The effect of the microstructure evolution on mechanical properties of the Fe-32Cr-4Ni-4Cu model alloy after long-term thermal aging at 475 °C can be summarized as follows:

Through a TEM structure analysis, it is found that spinodal decomposition first occurs at the grain boundaries, and then proceeds from the grain boundaries to the grains with the extension of the thermal-aging time. Decomposition products appear as a black-and-white lamellar structure in the TEM micrograph. The Cu-rich phase precipitated in the early stage of thermal aging (300-h thermal aging) has the same crystal structure as the matrix, which is a BCC structure. When thermal aging continues, the crystal structure of the Cu-rich phase changes from the BCC structure to a multi-twin 9R structure or 2H structure, and finally to a stable FCC structure. The precipitated Cu-rich phase and Cr-rich phase (α') generated by spinodal decomposition play a major role in hardening, compared with the model alloy. The quantity and size of the Cu-rich phase precipitated in the early stage of thermal aging have a great impact on the hardness of the alloy. After the continuous thermal aging up to 1000 h, the hardness of the alloy is affected by Cr-rich α'. The results of the oscillographic impact test show that the toughness of the model alloy after thermal aging at 475 °C is poor compared with the sample without thermal aging, which is mainly affected by the precipitation of the Cu-rich phase during thermal aging. The fracture mechanism of the model alloy after thermal aging at 475 °C is brittle fracture.

Acknowledgment

This work was supported by the Liaoning Provincial Applied Basic Research Project (2023JH2/101300233) in 2023; National Natural Science Foundation of China (No. 12375305); Basic Research Projects of Higher Education Institutions in Liaoning Province in 2023 (JYTZD20230004, JYTMS20230193); and Liaoning Provincial College Students' Innovation and Entrepreneurship Training Program in 2022 (S202210144062).

5 REFERENCES

[1] J. Wang, H. Zou, X. Y. Wu, Effect of long-term aging at 350 °C on dynamic fracture toughness of 17-4PH stainless steel, Atomic Energy Science and Technology, 02 (**2006**), 243–248, doi:10.1300/J064v28n01_10

[2] J. Wang, Performance study of 17-4PH stainless steel for nuclear reactor, Sichuan University, 2007, doi:10.7666/d.y1213057

[3] H. Zou, J. Wang, C. Li, R. L. Zuo, Transmission electron microscope observation of the long-term aging structure evolution of 17-4PH stainless steel at 350 °C, Nuclear Power Engineering, 04 (**2005**), 397–401+409, doi:10.1016/j.nucengdes.2006.03.017

[4] J. Wang, H. Zou, C. Li, Relationship of microstructure transformation and hardening behavior of type 17-4 PH stainless steel, Journal of University of Science and Technology Beijing, 13 (**2006**), 235–239, doi:10.1016/S1005-8850(06)60050-9

[5] C. N. Hsiao, C. S. Chiou, J. R. Yang, Aging reactions in a 17-4 PH stainless steel, Materials Chemistry and Physics, 74 (**2002**), 134–142, doi:10.1016/S0254-0584(01)00460-6

[6] Y. Y. Gao, Effect of thermal aging under simulated working conditions on dynamic mechanical properties of stainless steel for nuclear power, Xi'an University of Technology, 2018, doi:CNKI:CDMD:2.1018.710024

[7] N. Cao, Study on thermal aging mechanism of stainless steel for nuclear power main pipeline at different temperatures, Xi'an University of Technology, 2019, doi:10.27391/d.cnki.gxagu.2019.000059

[8] Z. P. Wang, F. G. Wang, Z. T. Liu, Spinodal decomposition of thermal aging of Z3CN20.09M cast dual-phase steel, Journal of Xi'an University of Technology, 33 (**2013**), 643–647, doi:10.3969/j.issn.1673-9965.2013.08.010

[9] N. N. Li, Study on the interaction mechanism between nano-Cu-rich phase and dislocation in RPV simulation steel, Shandong University of Technology, 2019, doi:10.27276/d.cnki.gsdgc.2019.000019

[10] H. Xie, W. Wang, Precipitation characteristics of nano Cu-rich phase in low carbon low alloy steel, Metal Heat Treatment, 43 (**2018**), 72–76, doi:10.13251/j.issn.0254-6051.2018.02.014

[11] L. Feng, B. X. Zhou, J. C. Peng, RPV simulated complex crystal structure characterization of nano-Cu-rich precipitates in steel, Materials Engineering, 43 (**2015**), 80–86, doi:10.11868/j.issn.1001-4381.2015.07.014

[12] W. Wang, L. Wang, X. Y. Zhou, Effect of aging process on precipitation of Cu-rich clusters in reactor pressure vessel steel, Journal of Material Heat Treatment, 34 (**2013**), 114–119, doi:CNKI:SUN:JSCL.0.2013-12-021

[13] Z. P. Wang, F. G. Wang, Z. T. Liu, Spinodal decomposition of thermal aging of Z3CN20.09M cast dual-phase steel, Journal of Xi'an University of Technology, 33 (**2013**), 643–647, doi:10.3969/j.issn.1673-9965.2013.08.010

[14] Y. Sun, Q. B. Yu, Analysis of cleavage fracture mechanism and microstructure of low carbon steel, Journal of Kunming University of Science and Technology (Natural Science Edition), 36 (**2011**), 18–22, doi:CNKI:SUN:KMLG.0.2011-04-005